Short-time rheology and diffusion in suspensions of Yukawa-type colloidal particles

Marco Heinen, Adolfo J. Banchio, and Gerhard Nägele

Citation: J. Chem. Phys. **135**, 154504 (2011); doi: 10.1063/1.3646962
View online: http://dx.doi.org/10.1063/1.3646962
View Table of Contents: http://jcp.aip.org/resource/1/JCPSA6/v135/i15
Published by the American Institute of Physics.

Short-time rheology and diffusion in suspensions of Yukawa-type colloidal particles

Marco Heinen,[1,a)] Adolfo J. Banchio,[2] and Gerhard Nägele[1]
[1]*Institute of Complex Systems (ICS-3), Forschungszentrum Jülich, D-52425 Jülich, Germany*
[2]*FaMAF, Universidad Nacional de Córdoba, IFEG-CONICET, Ciudad Universitaria, 5000 Córdoba, Argentina*

(Received 8 August 2011; accepted 15 September 2011; published online 19 October 2011)

A comprehensive study is presented on the short-time dynamics in suspensions of charged colloidal spheres. The explored parameter space covers the major part of the fluid-state regime, with colloid concentrations extending up to the freezing transition. The particles are assumed to interact directly by a hard-core plus screened Coulomb potential, and indirectly by solvent-mediated hydrodynamic interactions. By comparison with accurate accelerated Stokesian Dynamics (ASD) simulations of the hydrodynamic function $H(q)$, and the high-frequency viscosity η_∞, we investigate the accuracy of two fast and easy-to-implement analytical schemes. The first scheme, referred to as the pairwise additive (PA) scheme, uses exact two-body hydrodynamic mobility tensors. It is in good agreement with the ASD simulations of $H(q)$ and η_∞, for smaller volume fractions up to about 10% and 20%, respectively. The second scheme is a hybrid method combining the virtues of the $\delta\gamma$ scheme by Beenakker and Mazur with those of the PA scheme. It leads to predictions in good agreement with the simulation data, for all considered concentrations, combining thus precision with computational efficiency. The hybrid method is used to test the accuracy of a generalized Stokes-Einstein (GSE) relation proposed by Kholodenko and Douglas, showing its severe violation in low salinity systems. For hard spheres, however, this GSE relation applies decently well. © *2011 American Institute of Physics*. [doi:10.1063/1.3646962]

I. INTRODUCTION

Charge-stabilized systems of globular Brownian particles are ubiquitously found over a large range of particle sizes, from large, micron-sized colloids[1–3] down to nanometer-sized proteins.[4–6] For many such systems, where van der Waals attractions are to a good approximation negligible, the pair interactions can be described to good accuracy by a hard-sphere plus repulsive Yukawa (HSY)-type pair potential, of range determined by the ionic strength of dissolved co- and counterions. The HSY model spans the range from neutral hard spheres, corresponding to zero screening length or vanishing Yukawa potential strength, to long-range electric repulsion occurring in low-salinity systems with large screening length. In most applications of the HSY model to charged colloids, the Yukawa-tail of the pair interaction is described by the electrostatic part of the Derjaguin-Landau-Verwey-Overbeck (DLVO) potential.[7]

In experimental data analysis and many theoretical applications, easy-to-implement analytic methods are on demand that allow to calculate, with good accuracy, short-time dynamic properties, such as diffusion coefficients and high-frequency viscosities with a minimal computational effort. Short-time diffusion properties are routinely measured in dynamic light scattering,[8,9] x-ray photon correlation spectroscopy,[2,10] and neutron spin echo[11,12] experiments. The high-frequency viscosity η_∞ is probed experimentally using torsional viscometers, or on employing approximate generalized Stokes-Einstein (GSE) relations, which relate η_∞ to a diffusion property.[13,14]

Fast and accurate theoretical methods for calculating dynamic properties are valuable in particular for an extensive data analysis, where different system parameters such as concentration, salt content, particle size and charge, *p*H-value, and solvent properties, are considered in a broad range of values.

We point out here that short-time dynamic properties are of relevance not only in their own right. They are also required as input to theories describing colloidal long-time dynamics such as mode-coupling and dynamic density functional theory approaches.

A particular challenge in the development of analytic methods is the inclusion of the long-ranged, and for more concentrated systems non-pairwise additive, hydrodynamic interactions (HIs), which essentially influence the dynamic properties in their short-time behavior. Due to their complexity, the inclusion of HIs constitutes a severe bottleneck in Brownian dynamics simulations. The account of many-body HIs in analytic methods is only possible by introducing approximations. For this reason, it is of prime importance to assess the overall accuracy of analytic methods, by the comparison to precise benchmark results obtained from computationally elaborate dynamic computer simulations.

In this paper, we discuss the pros and cons of two easy-to-implement analytic methods of calculating short-time dynamic properties, such as the wavenumber-dependent

a)Electronic mail: m.heinen@fz-juelich.de.

hydrodynamic function $H(q)$, and the low shear-rate, high-frequency limiting viscosity η_∞. The first method, referred to as the pairwise additive (PA) scheme, uses exact two-body hydrodynamic mobility tensors including the lubrication part, but it fully disregards three-body and higher-order hydrodynamic contributions. The second scheme is a hybrid method combing the virtues of Beenakker and Mazur's so-called $\delta\gamma$-scheme approach for $H(q)$ (Refs. 15 and 16) and η_∞,[17] with those of the PA scheme, and precise known results for the special case of neutral hard spheres. The $\delta\gamma$ scheme accounts for many-body HI contributions in an approximate way. We present the two methods in a self-contained way, allowing for their easy implementation. Both methods require the static structure factor, $S(q)$, or equivalently the radial distribution function (rdf) $g(r)$, as the only input. We calculate this static input using our recently developed analytic modified penetrating-background corrected rescaled mean spherical approximation (MPB-RMSA) scheme,[18,19] which allows for a fast and accurate evaluation of the HSY pair-structure functions.

The accuracy of both methods for calculating $H(q)$ and η_∞ is assessed through comparison with a large number of simulation results, representative of the full fluid-state regime, which we have obtained using accelerated Stokesian dynamics simulations. The usefulness of the $\delta\gamma$ scheme-based hybrid method is illustrated by testing the validity of three generalized Stokes-Einstein relations.

The paper is organized as follows. Section II explains the essentials of the HSY model, and the MPB-RMSA method of calculating $S(q)$. The theoretical background on the short-time dynamics of interacting colloidal particles is included in Sec. III, and Sec. IV explains the employed methods of calculating short-time dynamic properties. Our results for $H(q)$, η_∞ and additional related short-time properties are summarized in Sec. V. Section VI includes the test of GSEs, notably that proposed by Kholodenko and Douglas. Our conclusions are given in Sec. VII.

II. PAIR-POTENTIAL AND STATIC STRUCTURE

The present study is concerned with charged spherical colloidal particles that interact directly via the HSY- type pair potential,

$$\beta u(x) = \begin{cases} \infty, & x = r/\sigma \le 1, \\ \gamma \dfrac{e^{-kx}}{x}, & x > 1. \end{cases} \tag{1}$$

The coupling amplitude γ and the screening parameter k are given by

$$\gamma = \frac{L_B}{\sigma}\left(\frac{Ze^{k/2}}{1+k/2}\right)^2, \tag{2}$$

$$k^2 = \frac{L_B/\sigma}{1-\phi}(24\phi|Z| + 8\pi n_s\sigma^3). \tag{3}$$

This constitutes the repulsive part of the DLVO potential.[7] Here, $\beta = 1/k_BT$, with Boltzmann constant k_B, absolute temperature T, colloidal hard-core diameter σ, solvent-characteristic Bjerrum length $L_B = \beta e^2/\epsilon$ in Gaussian units, proton elementary charge e, and solvent dielectric constant ϵ. In the DLVO expressions in Eqs. (2) and (3), γ and k are determined by the number concentration of monovalent (salt) coions, n_s, the effective colloid charge, Ze, and the colloid volume fraction, ϕ. The square of k is a sum of two contributions, namely, $k_c^2 = 24\phi|Z|L_B/[\sigma(1-\phi)]$ and $k_s^2 = 8\pi n_s\sigma^2 L_B/(1-\phi)$. The first one, k_c^2, describes the screening influence of monovalent counterions released from the colloid surfaces, and the second one, k_s^2, accounts for the screening influence of monovalent electrolyte ions arising from added salt. As shown in Refs. 20 and 21, the factor $1/(1-\phi)$ in Eq. (3) corrects for the free volume accessible to the microions in presence of impermeable colloidal spheres.

In recent work,[18,19] we have introduced a semi-analytic Ornstein-Zernike integral equation scheme[22] for calculating equilibrium pair-distribution functions, denoted as the MPB-RMSA. This computationally highly effective method allows for calculating the static structure factor, $S(q)$, as a function of the scattering wavenumber q, for particles interacting by the HSY pair potential given in Eq. (1). For a detailed derivation and validation of the MPB-RMSA, we refer to Refs. 18 and 19. In the limiting case of neutral hard spheres (HS), attained for $\gamma = 0$ ($Z = 0$) or $k \to \infty$ (very large n_s), the MPB-RMSA reduces to the analytic Percus-Yevick solution.[24,25]

Most of the results on short-time properties discussed in this work are for the parameters $L_B = 5.617$ nm, $\sigma = 200$ nm, and $Z = 100$, representative of strongly charged colloidal spheres suspended in an organic solvent. Numerous MPB-RMSA, Rogers-Young scheme,[23] and MC simulation results for $S(q)$ and $g(r)$ using these parameters are included in Figs. 2, 3, and 4 of Ref. 18. These results cover basically the whole fluid regime, with ϕ ranging from 10^{-4} to 0.15, and n_s from 0 to 10^{-4} M. For conciseness, and since these results for $S(q)$ and $g(r)$ have been published already, we refrain from replotting them in the present work.

III. SHORT-TIME DYNAMIC PROPERTIES

For characterizing the colloidal short-time regime, one considers the momentum relaxation time, $\tau_B = m/(3\pi\eta_0\sigma)$, the time scale $\tau_H = \sigma^2\rho_S/(4\eta_0)$ of hydrodynamic vorticity diffusion, and the interaction time $\tau_I = \sigma^2/(4d_0)$,[26,27] where m is the mass of a colloidal sphere, $d_0 = k_BT/(3\pi\eta_0\sigma)$ is the translational free diffusion coefficient for stick hydrodynamic surface boundaries, and ρ_S and η_0 are the mass density and shear viscosity of the suspending Newtonian solvent, respectively. For a coarse-grained time-resolution where $t \gg \tau_B \sim \tau_H$, the motion of a colloidal particle is erratic and overdamped. In the present work we focus on the colloidal short-time regime $\tau_B \ll t \ll \tau_I$, during which a particle has moved a tiny fraction of its size only. This allows for calculating short-time properties using pure equilibrium averages.

Diffusion properties can be measured by a variety of scattering techniques, which commonly determine the dynamic structure factor,[22]

$$S(q,t) = \left\langle \frac{1}{N}\sum_{l,j=1}^{N} \exp\{i\mathbf{q}\cdot[\mathbf{R}_l(0) - \mathbf{R}_j(t)]\} \right\rangle, \tag{4}$$

as a function of scattering wavenumber q and correlation time t. The brackets, $\langle \dots \rangle$, denote an equilibrium ensemble average, including the thermodynamic limit $N \to \infty$ and system volume $V \to \infty$, with $n = N/V$ fixed, which characterizes a macroscopic system. N is the number of colloid particles in the scattering volume, $\mathbf{q}$ is the scattering wave vector, and $\mathbf{R}_n(t)$ is the position vector pointing to the center of the nth colloidal particle at time t. On the colloidal short-time scale, $S(q, t)$ decays exponentially according to[8]

$$\frac{S(q,t)}{S(q)} = \exp[-q^2 D(q) t], \tag{5}$$

where $D(q)$ is the wavenumber-dependent short-time diffusion function. A statistical-mechanical expression for $D(q)$ follows from the generalized Smoluchowski equation in the form of the ratio[26–28]

$$D(q) = d_0 \frac{H(q)}{S(q)}, \tag{6}$$

of the hydrodynamic function

$$H(q) = \left\langle \frac{k_B T}{N d_0} \sum_{l,j=1}^{N} \hat{\mathbf{q}} \cdot \boldsymbol{\mu}_{lj}^{tt}(\mathbf{R}^N) \cdot \hat{\mathbf{q}} \exp\{i\mathbf{q} \cdot [\mathbf{R}_l - \mathbf{R}_j]\} \right\rangle, \tag{7}$$

and the static structure factor $S(q) = S(q, t = 0)$. Here, $\hat{\mathbf{q}}$ is the unit vector in the direction of $\mathbf{q}$, and $\boldsymbol{\mu}_{lj}^{tt}(\mathbf{R}^N)$ is a translational mobility tensor linearly relating the hydrodynamic force on a sphere j to the translational velocity of a sphere l. This mobility depends in general on the instantaneous positions, $\mathbf{R}^N$, of all N particles through the specified hydrodynamic boundary conditions. In this work, stick hydrodynamic boundary conditions are assumed throughout. The positive-valued hydrodynamic function $H(q)$ is a measure of the influence of HIs on short-time diffusion. In the (hypothetical) case of hydrodynamically non-interacting particles, $H(q) \equiv 1$, independent of q. The hydrodynamic function can be interpreted as the reduced short-time generalized mean sedimentation velocity measured in a homogeneous suspension subject to a weak force field collinear with $\mathbf{q}$ and oscillating spatially as $\cos(\mathbf{q} \cdot \mathbf{r})$. Hence,

$$\lim_{q \to 0} H(q) = \frac{U_{\text{sed}}}{U_0} \equiv K \tag{8}$$

is equal to the concentration-dependent (short-time) sedimentation velocity, U_{sed}, of a slowly settling homogeneous suspension of spheres in units of the sedimentation velocity, U_0, at infinite dilution.

The function $H(q)$ can be expressed as the sum,

$$H(q) = \frac{d_S}{d_0} + H^d(q), \tag{9}$$

of a q-dependent distinct part, $H^d(q)$, which vanishes for $q \to \infty$, and a self-part equal to the reduced short-time translational self-diffusion coefficient d_s/d_0. The diffusion coefficient d_s is equal to the short-time slope of the mean-squared displacement, $W(t) = 1/6\langle[\mathbf{R}(t) - \mathbf{R}(0)]^2\rangle$, of a colloidal particle.[27]

Two additional diffusion coefficients related to $D(q)$ are the short-time collective diffusion coefficient $d_c = d_0 K/S(q \to 0)$, and the short-time cage diffusion coefficient $d_{\text{cge}} = D(q_m)$. These two coefficients characterize the decay rates, respectively, of thermally induced concentration fluctuations of macroscopic wavelengths, and of a wavelength related to the size, $2\pi/q_m$, of the dynamic next-neighbor cage formed around a particle.

So far only diffusion properties have been discussed. A rheological short-time property is the high-frequency limiting viscosity, η_∞, which linearly relates the average deviatoric suspension shear stress to the applied rate of strain in a low-amplitude, oscillatory shear experiment with frequency $\omega \gg 1/\tau_I$. The statistical-mechanical expression for η_∞ is[29]

$$\eta_\infty = \eta_0 + \sum_{\alpha,\beta=1}^{3} \left\langle \frac{1}{10V} \sum_{l,j=1}^{N} \mu_{lj\ \alpha\beta\beta\alpha}^{dd}(\mathbf{R}^N) \right\rangle, \tag{10}$$

invoking the Cartesian components, $\mu_{lj\ \alpha\beta\beta\alpha}^{dd}$, of the $3 \times 3 \times 3 \times 3$ dipole-dipole mobility tensor $\boldsymbol{\mu}_{lj}^{dd}$, that relates the symmetric hydrodynamic force dipole moment tensor of sphere l to the rate of strain tensor related to sphere j. For stick hydrodynamic boundary conditions, $\eta_\infty = \eta_0[1 + 2.5\phi + \mathcal{O}(\phi^2)]$, where η_0 is the solvent viscosity. The $\mathcal{O}(\phi^2)$ contribution is due to particle interactions. Note here that $\langle \dots \rangle$ describes an equilibrium average with respect to the unsheared system. Direct interactions affect η_∞ only through their influence on the equilibrium particle distribution.

The great difficulty in evaluating Eqs. (7) and (10) to obtain $H(q)$ and η_∞, respectively, lies in the calculation of the hydrodynamic tensors $\boldsymbol{\mu}_{lj}^{tt}(\mathbf{R}^N)$ and $\boldsymbol{\mu}_{lj}^{dd}(\mathbf{R}^N)$, and in the associated many-particle average. Except for numerically expensive simulations,[14,30–32] it is practically impossible to gain numerically precise results for concentrated systems. In searching for methods which allow to calculate $H(q)$ and η_∞ to decent accuracy with moderate numerical effort, one has to resort to approximate methods. Two of these methods, namely, the so-called PA approximation, and the $\delta\gamma$-scheme by Beenakker and Mazur supplemented by a so-called self-part correction, are discussed in Sec. IV. The methods are presented in a self-contained way to facilitate their implementation by an interested reader. Both methods have in common that they require $S(q)$, or equivalently $g(r)$, as the only input. The pros and cons of both methods are assessed in comparison to elaborate computer simulations.

IV. COMPUTATIONAL METHODS

A. Pairwise additive approximation

In the PA approximation, the N-particle translational mobility tensors, $\boldsymbol{\mu}_{lj}^{tt}(\mathbf{R}^N)$, are approximated by the sum of two-body mobilities according to

$$\frac{k_B T}{d_0} \boldsymbol{\mu}_{lj}^{tt}(\mathbf{R}^N)\Big|_{\text{PA}} = \delta_{lj} \left[1 + \sum_{n \neq l}^{N} \mathbf{a}_{11}(\mathbf{R}_l - \mathbf{R}_n) \right] + (1 - \delta_{lj}) \mathbf{a}_{12}(\mathbf{R}_l - \mathbf{R}_j). \tag{11}$$

The 3×3 mobility tensor $1 + \mathbf{a}_{11}$ relates, for an isolated pair of particles in a quiescent fluid, the force on particle 1 to its own velocity. Correspondingly, $\mathbf{a}_{12}$ relates the

force on particle 2 to the velocity of particle 1. The axial symmetry of the two-sphere problem allows to split the reduced mobilities into longitudinal and transverse components,

$$\delta_{ij}1 + \mathbf{a}_{ij}(\mathbf{r}) = x^a_{ij}(r)\hat{\mathbf{r}}\hat{\mathbf{r}} + y^a_{ij}(r)\left[1 - \hat{\mathbf{r}}\hat{\mathbf{r}}\right], \tag{12}$$

where we use the notation from Ref. 33. The mobility components $x^a_{ij}(r)$ and $y^a_{ij}(r)$ can be expanded analytically in powers of $\sigma/r = 1/x$ using recursion formulas.[34]

In a homogeneous fluid system, the ensemble average of a function f depending on two particle coordinates can be expressed in the thermodynamic limit as

$$\langle f(\mathbf{R}_l - \mathbf{R}_j)\rangle = \lim_{V\to\infty}\frac{1}{V}\int_V d\mathbf{r} g(r) f(\mathbf{r}). \tag{13}$$

The combination of Eqs. (7), (11), and (13) leads to the following PA results for d_S,

$$\left.\frac{d_S}{d_0}\right|_{\mathrm{PA}} = 1 + 8\phi\int_1^\infty dx x^2 g(x)\left[x^a_{11}(x) + 2y^a_{11}(x) - 3\right], \tag{14}$$

and for the distinct part of the hydrodynamic function,

$$\begin{aligned} H^d(y)|_{\mathrm{PA}} = &-15\phi\frac{j_1(y)}{y} + 18\phi\int_1^\infty dx x h(x) \\ &\times\left[j_0(xy) - \frac{j_1(xy)}{xy} + \frac{j_2(xy)}{6x^2}\right] \\ &+ 24\phi\int_1^\infty dx x^2 g(x)\tilde{y}^a_{12}(x) j_0(xy) \\ &+ 24\phi\int_1^\infty dx x^2 g(x)\left[\tilde{x}^a_{12}(x) - \tilde{y}^a_{12}(x)\right] \\ &\times\left[\frac{j_1(xy)}{xy} - j_2(xy)\right]. \end{aligned} \tag{15}$$

Here, $y = q\sigma$ is the diameter-scaled wavenumber, j_n is the spherical Bessel function of first kind and order n, and h is the total correlation function defined by $h(x) = g(x) - 1$.

We have introduced here the short-range mobility parts

$$\tilde{x}^a_{12}(x) = x^a_{12}(x) - 3/4x^{-1} + 1/8x^{-3}, \tag{16}$$

$$\tilde{y}^a_{12}(x) = y^a_{12}(x) - 3/8x^{-1} - 1/16x^{-3}, \tag{17}$$

which include all terms in the series expansion except for the far-field terms up to the dipolar (Rotne-Prager) level, which are subtracted off.

Analogous to the translational diffusivity tensors, the dipole-dipole mobility tensors are approximated in the PA scheme by their self and distinct two-body contributions $\boldsymbol{\mu}^{dd(2)}_{11}(\mathbf{r})$, $\boldsymbol{\mu}^{dd(2)}_{12}(\mathbf{r})$, respectively. In hydrodynamically semidilute suspensions, the high-frequency viscosity of colloidal spheres at low shear-rate is then obtained from[14,35,36]

$$\frac{\eta_\infty}{\eta_0} = 1 + \frac{5}{2}\phi(1+\phi) + 60\phi^2\int_1^\infty dx x^2 g(x) J(x), \tag{18}$$

where the rapidly decaying two-body shear mobility function, $J(x)$, accounts for the two-body HIs. For stick hydrodynamic boundary conditions, $J(x) = 15/128x^{-6} + \mathcal{O}(x^{-8})$.

For pair-distances $x > 3$, we use explicit analytic expansions up to $\mathcal{O}(x^{-20})$, given in Ref. 34 for the two-body mobility functions x^a_{ij} and y^a_{ij}, and the leading-order far-field expression, $J(x) = 15/128x^{-6}$, for the shear mobility function. Since the expansions in $1/x$ converge slowly at small separations, we employ accurate numerical tables for $x < 3$, which in particular account for lubrication at near-contact distances. The tables are based on recursion expressions and a lubrication analysis given in Ref. 33.

Using the zeroth-order concentration-expansion for the rdf of hard spheres given by $g^{\mathrm{HS}}(x) = \Theta(x-1) + \mathcal{O}(\phi)$, with Θ denoting the unit step function, we have checked that our PA code precisely reproduces the truncated virial expressions,

$$\frac{d^{\mathrm{HS}}_s}{d_0} = 1 - 1.8315\phi + \mathcal{O}(\phi^2), \tag{19}$$

$$K^{\mathrm{HS}} = 1 - 6.546\phi + \mathcal{O}(\phi^2), \tag{20}$$

$$\frac{\eta^{\mathrm{HS}}_\infty}{\eta_0} = 1 + \frac{5}{2}\phi + 5.0023\phi^2 + \mathcal{O}(\phi^3), \tag{21}$$

which were obtained in Refs. 37–39 using a mobility series expansion including terms up to $\mathcal{O}(x^{-1000})$, and a lubrication correction.

All PA results for $H(q)$ and η_∞ discussed in this paper are based on Eqs. (14), (15), and (18), with $g(x)$ computed in MPB-RMSA. Dynamical properties predicted by the PA scheme are exact to linear order in ϕ. Thus, the PA scheme is especially well-suited for hydrodynamically, but not necessarily structurally, dilute systems. Charge-stabilized suspensions at low salinity and concentration, where near-contact configurations are very unlikely, are prime examples of hydrodynamically dilute, but structurally ordered systems, showing pronounced oscillations in $S(q)$ and $g(r)$.

Moreover, the PA scheme can be used to check the accuracy of other approximate schemes, such as the (self-part corrected) $\delta\gamma$ scheme, in the low concentration regime. At larger volume fractions, however, and for diffusion properties like d_c and K, where non-pairwise additive HIs are particularly influential, the PA approximation is bound to fail. Note that, while in the present work particles with stick hydrodynamic boundary conditions are considered, the PA scheme can be easily generalized to porous particles, and particles with slip-stick boundary conditions, simply by using the corresponding two-body mobility functions given, e.g., in Ref. 34.

B. $\delta\gamma$-method by Beenakker and Mazur

Different from the PA scheme, which cannot be applied to concentrated systems, the renormalized concentration fluctuation (termed $\delta\gamma$) expansion method of Beenakker and Mazur[15,17] is applicable to fluid disordered systems also at large values of ϕ, where three-body and higher-order HI contributions are important. The $\delta\gamma$ method is an effective medium approach based on a partial resummation of many-body HI contributions. While applicable to all ϕ, its results for $H(q)$ and η_∞ reveal moderate inaccuracies at all concentrations, including the very dilute regime where the PA approach becomes exact. These inaccuracies can be partially

traced back to the approximate expressions of $\boldsymbol{\mu}_{lj}^{tt}(\mathbf{R}^N)$ and $\boldsymbol{\mu}_{lj}^{dd}(\mathbf{R}^N)$ used in the derivation of the $\delta\gamma$-scheme where, in particular, lubrication corrections are disregarded. Higher order terms in the $\delta\gamma$ expansion require as input static correlation functions of increasing order (pair, triplet, and so on) with swiftly increasing difficulties in their evaluation.

In the present study, we use the easy-to-implement standard version of the $\delta\gamma$ method for which (like for the PA scheme) only $S(q)$ is required as input, with the latter calculated here using the MPB-RMSA scheme. This is the zeroth-order $\delta\gamma$ approximation regarding $H(q)$, and the second-order $\delta\gamma$ approximation regarding η_∞.

The zeroth-order $\delta\gamma$ scheme for $H(q)$ has been applied in the past both to neutral and charged colloidal particles, but the second-order $\delta\gamma$ scheme for η_∞ was used so far for neutral hard spheres only. To our knowledge, the present work provides the first test of the $\delta\gamma$ scheme for charged, Yukawa-type particles.

The zeroth-order $\delta\gamma$-scheme expression for $H(q)$ consists of a microstructure-independent part,

$$\left.\frac{d_s(\phi)}{d_0}\right|_{\delta\gamma} = \frac{2}{\pi}\int_0^\infty dy\left[\frac{\sin(y)}{y}\right]^2\cdot[1+\phi S_{\gamma_0}(y)]^{-1}, \tag{22}$$

and a structure factor dependent distinct hydrodynamic function part,

$$H^d(y)|_{\delta\gamma} = \frac{3}{2\pi}\int_0^\infty dy'\left[\frac{\sin(y')}{y'}\right]^2\cdot[1+\phi S_{\gamma_0}(y')]^{-1} \times\int_{-1}^1 d\mu(1-\mu^2)[S(|\mathbf{q}-\mathbf{q}'|)-1], \tag{23}$$

where μ is the cosine of the angle between $\mathbf{q}$ and $\mathbf{q}'$.[40] The function $S_{\gamma_0}(y)$, which should not be confused with the static structure factor, is given in Refs. 15 and 40 as an infinite sum of wavenumber-dependent contributions with interrelated scalar coefficients $\gamma_0^{(n)}$, $n=0\ldots\infty$. Numerical results for $\gamma_0^{(n)}$ obtained from a computation truncated at $n=5$ have been given in Table I of the original paper by Beenakker and Mazur.[15] Taking advantage of the nowadays available computing power, we have been able to extend these earlier computations to more terms with truncations at $n=10$ and 15. However, our more accurate results for $\gamma_0^{(n)}$ differ from the original results by Beenakker and Mazur by no more than 3%, and the differences in $H^d(y)|_{\delta\gamma}$, $d_s(\phi)|_{\delta\gamma}$, and $\eta_\infty|_{\delta\gamma}$ are negligible for all practical purposes.

The high-frequency limiting viscosity in the second-order $\delta\gamma$-scheme is given by[17]

$$\left.\frac{\eta_\infty}{\eta_0}\right|_{\delta\gamma} = \frac{1}{\lambda_0+\lambda_2}, \tag{24}$$

$$\lambda_0 = \left[1+\frac{5}{2}\phi\tilde{\gamma}_0^{(2)}\right]^{-1} = 1-\frac{5}{2}\phi+\frac{215}{168}\phi^2+\mathcal{O}(\phi^3), \tag{25}$$

$$\lambda_2 = \frac{30\phi}{4\pi}\left[\lambda_0\tilde{\gamma}_0^{(2)}\right]^2\int_0^\infty dy\,\frac{j_1^2(y/2)\left[S(y/\sigma)-1\right]}{1+\phi S_{\gamma_0}(y/2)}, \tag{26}$$

where $\tilde{\gamma}_0^{(2)}=\gamma_0^{(2)}/n=1+167/84\phi+\mathcal{O}(\phi^2)$.

Insertion of the low-concentration form, $S^{\mathrm{HS}}(y)=1-24\phi j_1(y)/y+\mathcal{O}(\phi^2)$, of the static structure factor of neutral hard spheres into Eqs. (22), (23), and (24) gives, after a straightforward calculation, the first-order virial expansion results

$$\left.\frac{d_s^{\mathrm{HS}}}{d_0}\right|_{\delta\gamma}+\mathcal{O}(\phi^2) = 1-\frac{131}{56}\phi\approx 1-2.339\phi, \tag{27}$$

$$K^{\mathrm{HS}}|_{\delta\gamma}+\mathcal{O}(\phi^2) = 1-\frac{411}{56}\phi\approx 1-7.339\phi, \tag{28}$$

$$\left.\frac{\eta_\infty^{\mathrm{HS}}}{\eta_0}\right|_{\delta\gamma}+\mathcal{O}(\phi^3) = 1+\frac{5}{2}\phi+\frac{1255}{168}\phi^2 \approx 1+\frac{5}{2}\phi+7.47\phi^2, \tag{29}$$

predicted by the $\delta\gamma$ scheme. The magnitudes of the linear virial coefficients of d_s^{HS}/d_0 and K^{HS}, and of the quadratic coefficient of $\eta_\infty^{\mathrm{HS}}/\eta_0$, overestimate the precise values given in Eqs. (19), (20), and (21) by 28%, 12%, and 49%, respectively. The effect of HIs on these quantities on the pair-level is thus overestimated by the $\delta\gamma$ scheme. Clearly, the PA scheme is the method of choice when very dilute systems are considered. We note further that $H_{\delta\gamma}^d(q\to 0)=-5\phi+\mathcal{O}(\phi^2)$ for hard spheres, a result quite close to the exact result of $H^d(q\to 0)=-4.714\phi+\mathcal{O}(\phi^2)$. This indicates that the zeroth-order $\delta\gamma$ scheme is in general a better approximation for the distinct part, $H^d(q)$, of the hydrodynamic function than for its self-part d_s.

Interestingly enough, the first-order in ϕ result for $H^d(q\to 0)$ for hard-spheres predicted by the $\delta\gamma$-scheme, is identical to the one obtained from the Rotne-Prager (RP) approximation of the HIs, where only the leading order monopole and dipole terms in the $1/x$ expansion of $\boldsymbol{\mu}_{lj}^{tt}$ are retained. For hard spheres, the first-order virial expansion result, $H(q_m)=1-1.35\phi$, for the principal peak height of $H(q)$ remains valid to high accuracy up to the volume fraction $\phi_f=0.494$ at freezing,[14] whereas in the RP approximation, peak values of $H(q)$ larger than one are predicted. The main reason for this failure of the RP approximation lies in its prediction of $d_s=d_0$ at all ϕ, whereas the actual d_s of hard spheres is significantly decreasing with increasing ϕ, down to the value $d_s^{\mathrm{HS}}(\phi_f)\approx 0.2d_0$ at freezing.

In low-salinity charge-stabilized systems at low concentrations, where $q_m\sigma\approx 2\pi\sigma n^{1/3}\ll 1$, the $\delta\gamma$-scheme gives predictions for $H^d(q)$ close to those by the RP approximation. Indeed, these are precisely the systems where the RP approximation can be expected to perform well, explaining in part the overall success of the $\delta\gamma$ scheme in making reliable predictions for the distinct part of $H(q)$ of charge-stabilized systems.

C. Self-part corrected $\delta\gamma$-scheme

The key observation regarding the zeroth-order $\delta\gamma$ expression for $H^d(q)$, which depends on $S(q)$ only, is that it gives overall good results both for neutral and charged Yukawa-type spheres. In contrast, the zeroth-order $\delta\gamma$ expansion for

d_s in Eq. (22) depends on ϕ only, independent of the employed pair-potential. Comparison with accelerated Stokesian Dynamics (ASD) simulation results,[14] and experimental data for d_s for charged colloids,[9,41] shows that Eq. (22) is a decent approximation of d_s for neutral hard spheres only.

The self-diffusion coefficient, $d_s(\phi)$, of charged spheres is in fact larger than the one for neutral spheres at the same ϕ,[42] since for the latter near contact configurations are more likely. Using leading-order far-field mobilities applicable to strongly charged colloids characterized by $q_m \propto \phi^{1/3}$, one finds for $\phi \lesssim 0.1$ a power-law dependence of d_s according to $d_s/d_0 \simeq 1 - a_t\phi^{4/3}$,[26,42–45] differing qualitatively from the regular hard-sphere virial result in Eq. (19). The coefficient $a_t \simeq 2.5 - 2.9$ in the fractional power law varies to a certain extent with the particle size and charge.

For suspensions of strongly charged spheres, where $\phi \lesssim 0.15$, it has been shown[9] that the PA result for d_s in Eq. (14) is in better agreement with ASD simulation results, and experimental data, than the corresponding $\delta\gamma$-scheme result based on Eq. (22). For larger concentrations $\phi \gtrsim 0.15$, the PA scheme overestimates the slowing hydrodynamic influence on d_s, since it does not account for the shielding of the HIs in pairs of particles by other intervening particles. Hydrodynamic shielding is a many-body effect which lowers the strength but not the range of the HIs. It should be distinguished from the screening of HIs by spatially fixed obstacles or boundaries which absorb momentum from the fluid, thereby causing a faster than $1/r$ decay of the flow perturbation created by a point-like force. The neglect of hydrodynamic shielding (i.e., three-body and higher-order HIs) by the PA scheme is more consequential for the sedimentation coefficient K than for d_s. To the former, the PA scheme is applicable to decent accuracy only up to $\phi \approx 0.1$,[9] whereas for larger ϕ, the coefficient K becomes increasingly underestimated. The coefficient d_s, on the other hand, is less sensitive to the neglect of higher-order HI contributions than K or d_c, since the leading-order far-field contributions to $x_{11}^a(x)$ and $y_{11}^a(x)$ are of $\mathcal{O}(x^{-4})$, i.e., of shorter range than the leading-order $\mathcal{O}(x^{-1})$ contributions to K.

As a simple improvement over the zeroth-order $\delta\gamma$ scheme for the $H(q)$ of charged particles, which preserves its analytic simplicity, we therefore use the self-part corrected expression,

$$H(y)|_{\delta\gamma_{\rm corr}} = \left.\frac{d_s}{d_0}\right|_{\rm PA} + H^d(y)\big|_{\delta\gamma}, \tag{30}$$

with d_s according to Eq. (14) and $H^d(q)$ according to Eq. (23), bearing in mind that $[d_s/d_0]_{\rm PA}$ becomes less reliable for $\phi \gtrsim 0.15$.

For the limiting case of neutral hard spheres at larger ϕ, it is therefore preferential to use in place of $[d_s/d_0]_{\rm PA}$ the accurate expression,

$$\left.\frac{d_s}{d_0}\right|^{HS} \approx 1 - 1.8315\phi(1 + 0.1195\phi - 0.70\phi^2) \tag{31}$$

which, for $\phi \leq 0.5$, agrees well with ASD (Ref. 14) and hydrodynamic force multipole[46] results, with an accuracy better than 3%. Note that the linear and quadratic order coefficients in Eq. (31) have been selected identical to the numerically precise values -1.8315 and $-0.219 = -1.8315 \times 0.1195$, for the respective virial coefficients given in Ref. 37. We have determined the cubic coefficient in Eq. (31) from a best fit to recent simulation results in Refs. 14 and 46. The coefficient 0.70 differs somewhat from the coefficient 0.65 in Ref. 46, where simulation results only up to $\phi \leq 0.45$ were considered.

A self-part corrected version of the $\delta\gamma$ scheme for $H(q)$ was used already in earlier applications, where d_s was considered simply as an adjustable parameter,[40] or in more recent work determined using elaborate ASD simulations.[14] For practical purposes, however, it is far more convenient to use the analytic d_s corrections in Eqs. (14), (30), and (31). In the present work, numerous ASD simulation results for $H(q)$, d_s, and η_∞ have been generated to provide precise benchmarks for assessing the accuracy of the proposed self-part corrected $\delta\gamma$ scheme.

While the $\delta\gamma$ scheme for $H(q)$ has been used already for charge-stabilized colloids, to our knowledge the application of the $\delta\gamma$ scheme for η_∞ in Eqs. (24)–(26) was restricted so far to colloidal hard spheres, where the predicted values for $\eta_\infty(\phi)$ are in good agreement, for $\phi \lesssim 0.4$, with experiments and simulation data. In Subsection V C, we are going to assess the performance of the $\delta\gamma$-scheme expression for the η_∞ of charged particles by comparison with ASD simulation data. Our analysis shows that the second-order $\delta\gamma$ contribution, $\lambda_2(\phi) < 0$, to η_∞/η_0 is only weakly dependent on the shape of the static structure factor. Moreover, the zeroth-order contribution, $\lambda_0(\phi) > 0$, which is only dependent on ϕ, dominates for small ϕ the contribution λ_2 in magnitude. As a consequence, the $\delta\gamma$-predicted values for η_∞ change only slightly when going from neutral to charged particles, whereas simulations, and experiments,[47] reveal significantly smaller viscosity values in particular at low salinities. Thus, the $\delta\gamma$-scheme result in Eqs. (24)–(26) applies to neutral hard spheres only. However, for the interesting case of low-salinity systems, where the viscosity differences to neutral spheres at equal concentration are largest, the $\delta\gamma$ scheme can be modified (corrected) in an ad-hoc way, according to

$$\left.\frac{\eta_\infty}{\eta_0}\right|_{\delta\gamma_{\rm corr}} = 1 + \frac{5}{2}\phi(1+\phi) - \frac{1}{\lambda_0} + \frac{1}{\lambda_0 + \lambda_2}. \tag{32}$$

The motivation for this correction follows from the PA expression in Eq. (18): For a low-salinity system of strongly repelling particles, one has the scaling $r_m \propto \phi^{-1/3}$ for the peak position, r_m, of the rdf, and $g(r \lesssim r_m) \approx 0$. Since $J(x)$ is of $\mathcal{O}(x^{-6})$, for these systems the integral in Eq. (18) is of $\mathcal{O}(\phi^3)$. Hence, to quadratic order in ϕ, η_∞ is determined basically by the microstructure-independent contribution, $1 + 2.5\phi(1 + \phi)$, according to Eq. (18).

In Eq. (32), we correct approximately for this limiting behavior of η_∞ by subtracting the structure-independent "self part," $1/\lambda_0$, from $[\eta_\infty/\eta_0]_{\delta\gamma}$, which renders the remainder of $\mathcal{O}(\phi^2)$ small, while adding the term $1 + 2.5\phi(1 + \phi)$. As we will show in Subsection V C, the so-corrected $\delta\gamma$ scheme is in very good agreement with the ASD viscosity data of low-salinity systems, even up to the freezing transition concentration. We point out here that Eq. (32) is restricted in its applicability to the low-salinity regime of strongly repelling particles. In contrast, the d_s-corrected $\delta\gamma$-scheme for $H(q)$ in

Eq. (30) applies to HSY systems for any set of system parameters $\{\gamma, k, \phi\}$, provided $\phi \lesssim 0.15$, including the crossover regime from neutral to deionized, highly charged particle systems. For neutral hard spheres, the (uncorrected) $\delta\gamma$ scheme for η_∞ performs quite well.

The design of a simple, corrected $\delta\gamma$ scheme which operates well for arbitrary $\{\gamma, k, \phi\}$, including systems of intermediate salinity, is obstructed by the limited separability of λ_0 and λ_2, and by significant many-body HI contributions for more concentrated systems of nearly hard-sphere-like particles at high salinity. For small values $\phi \lesssim 0.1$, the PA method can be used to produce reliable predictions of η_∞, for arbitrary salinities.

D. Accelerated Stokesian dynamics simulations

The simulation data for the $H(q)$ and η_∞ in HSY systems explored in this work, have been generated using an ASD simulation code. The details of the simulation method have been explained in Ref. 30. It allows to simulate short-time properties of a larger number of spheres, typically up to $N = 1000$, placed in a periodically replicated simulation box, allowing for improved statistics. Since short-time properties are obtained from single-time equilibrium averages, we have used equilibrium configurations generated using a Monte Carlo simulation method for charged spheres and a molecular dynamics algorithm for neutral hard spheres, with the many-sphere HIs accounted for using the ASD scheme. The computed hydrodynamic function, $H_N(q)$, shows a strong system-size dependence, even when N is not small. We therefore extrapolate $H_N(q)$ to the thermodynamic limit using the finite-size scaling correction,[48,49]

$$H(q) = H_N(q) + 1.76\, S(q) \frac{\eta_0}{\eta_\infty(\phi)} (\phi/N)^{1/3} , \qquad (33)$$

which, for $q \to 0$ and $q \to \infty$, includes the finite-size corrections for K and d_s, respectively. This finite-size correction formula was initially proposed by Ladd for hard spheres,[48,50,51] and has been subsequently applied also to charged spheres[14] and solvent-permeable particles.[31] As pointed out by Ladd,[48] and explained by Mo and Sangani,[49] η_∞ is not critically dependent on N so that finite size scaling extrapolation to $N \to \infty$ is not needed (see also Ref. 32). The simulation results discussed in Sec. V are obtained from averaging over 2000 configurations, for systems of typically $N = 512$ particles.

V. RESULTS

A. Diffusion properties of charged particles

In Fig. 1, theoretical and simulation results for $H(q)$ are shown for nine different systems with common system parameters $L_B = 5.617$ nm, $\sigma = 200$ nm, and $Z = 100$, representative of suspensions of highly charged colloidal spheres in an organic solvent. The parameters ϕ and n_s are varied, and assume values consisting of all permutations of $\phi = 0.055$, 0.105, and 0.15 and $n_s = 10^{-4}$, 10^{-5}, and 10^{-6} M. To facilitate the comparison of the different systems, identical axes scales are used in all nine panels, ordered with respect to ϕ, which increases from top to bottom, and n_s, decreasing from left to right. Thus, the strength of the interparticle correlations increases from left to right, and from top to bottom. Figure 1 serves for analyzing the accuracy of the corrected and uncorrected $\delta\gamma$ schemes, and of the PA scheme, in comparison to our finite-size corrected ASD results for $H(q)$.

The results for $H(q)$ obtained by all methods described in Sec. IV, are included in Fig. 1. Open symbols represent ASD simulation data, black dashed curves represent our PA results, blue dotted curves represent the zeroth-order $\delta\gamma$ scheme results, and red solid lines indicate the self-part corrected $\delta\gamma$ scheme predictions. The black and orange horizontal lines in each panel mark the reduced short-time self-diffusion coefficient, $d_s/d_0 = H(q \to \infty)$, obtained from the ASD simulations and the PA scheme, respectively. As the only input to the three analytic schemes, $S(q)$ and $g(r)$ of each system are obtained using our MPB-RMSA code. Except for $\phi = 0.105$, the MPB-RMSA results for $S(q)$ and $g(r)$ have been shown already in Figs. 3 and 4 of Ref. 18, and are therefore not included here.

The rightmost column of panels in Fig. 1 presents results for three systems of strongly charged particles with a very low residual, but experimentally still accessible, salt content. In the most concentrated system in panel (i), where $\phi = 0.15$ and $n_s = 10^{-6}$ M, a structure factor peak value $S(q_m) \approx 2.5$ is attained according to the MC simulations. The very same peak value is predicted by the MPB-RMSA and RY integral equation schemes. According to the empirical Hansen-Verlet freezing rule, the system in panel (i) is pretty close to the freezing transition point.[52–54]

The screening parameter k defined in Eq. (3) assumes rather low values of 2.67, 3.24, and 3.68 for the systems in panels (c), (f), and (i), with $k_c^2/k_s^2 = 1.1$, 2.1, and 3.0, respectively. The relatively large values for k_c^2/k_s^2 in these systems indicate that salt microions contribute little to the electrostatic screening, which instead is dominated by colloid-surface released counterions. Different from neutral hard spheres, where $H(q_m)$ decreases linearly with increasing ϕ, the hydrodynamic function peak heights of the three low-salinity systems depend non-monotonically on ϕ, with ASD values $H(q_m) = 1.13$, 1.17, and 1.15 for the systems in panels (c), (f), and (i), respectively. Such a non-monotonic ϕ-dependence of $H(q_m)$ is typical for low-salinity systems, as discussed in Refs. 14 and 55. The ASD results for the reduced self-diffusion coefficient, d_s/d_0, and the corrected $\delta\gamma$-scheme results for the sedimentation coefficient K in panels (c), (f), and (i), follow closely the concentration-scaling predictions $d_s/d_0 = 1 - a_t\phi^{4/3}$ and $K = 1 - a_s\phi^{1/3}$ given in Ref. 9, with $a_t = 2.63$ and with $a_s = 1.44$. The fractional exponents 4/3 and 1/3 can be traced back to the $\phi^{1/3}$ scaling in low-salinity systems, of the structure factor peak position, q_m. Note here that $H(q)$ has its principal peak at a wavenumber practically identical to the peak position of $S(q)$.

We proceed in our discussion with the systems in the leftmost column of panels. The salt concentration, $n_s = 10^{-4}$ M, of these systems is so large that the neutral hard-sphere limit is practically reached. The comparison with the $H(q)$ of genuine neutral hard spheres at volume fractions equal to those in panels (a), (d), and (g), shows relative differences of less than 6% in all three cases. The proximity

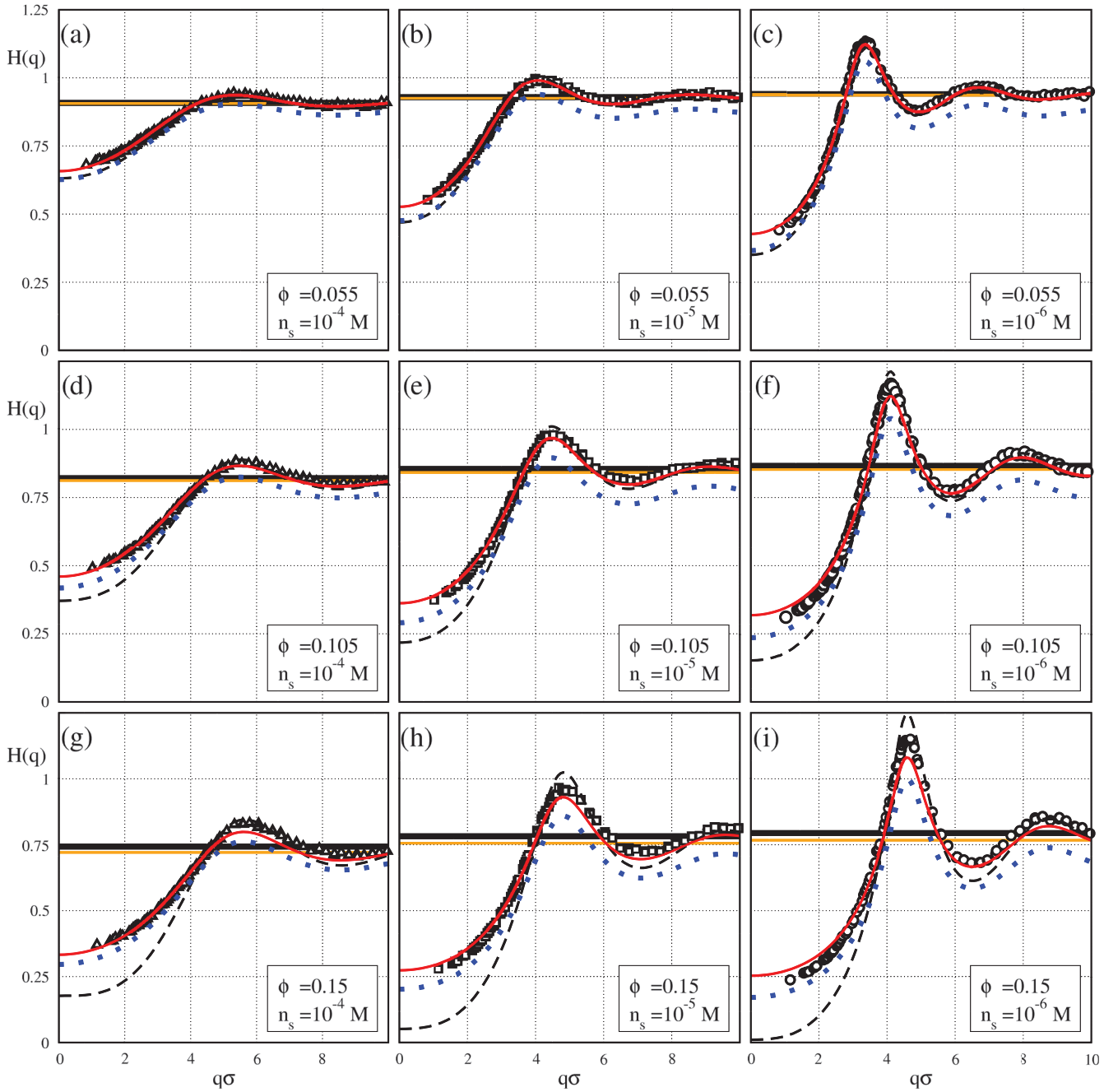

FIG. 1. Hydrodynamic function, $H(q)$, for charge-stabilized suspensions of volume fractions, ϕ, and salt concentrations, n_s, as indicated in each panel. The panels are ordered with respect to ϕ, which increases from top to bottom, and n_s, which decreases from left to right. Open symbols: ASD simulation data. Black dashed, blue dotted, and red solid curves: PA-scheme, $\delta\gamma$-scheme, and self-part corrected $\delta\gamma$-scheme results, respectively. In the latter scheme, the self-diffusion coefficient has been calculated using the PA scheme according to Eqs. (30) and (14). Horizontal black and orange lines mark the values for d_s/d_0 obtained from ASD simulation and PA-scheme calculations, respectively. Common system parameters are $L_B = 5.617$ nm, $\sigma = 200$ nm, and $Z = 100$.

to genuine neutral hard-sphere systems is manifest also in the large values, $k = 18.5$, 18.6, and 18.7, of the screening parameter, and in the small ratios $k_c^2/k_s^2 = 0.01, 0.02,$ and 0.03, for the systems in panels (a), (d), and (g), respectively.

For the smallest considered concentration $\phi = 0.055$ (top row of panels in Fig. 1), the differences in the respective $H(q)$ predicted by the analytic methods and the ASD simulations are very small. Since the PA scheme becomes exact at low ϕ, this illustrates that, despite their overall inaccuracies, the self-part corrected, and even the uncorrected $\delta\gamma$-scheme, can be used to obtain good estimates of $H(q)$ also for more dilute suspensions.

With increasing ϕ, pronounced differences are observed in Fig. 1 between the PA-scheme and ASD results for $H(q)$. This reflects the expected failure of the PA scheme in concentrated suspensions, where three-body and higher-order HI contributions become influential. The deviations of the PA-scheme results from the precise simulation data are most pronounced for the peak value $H(q_m)$, which is overestimated by the PA scheme, and in the sedimentation coefficient, $K = H(q$

$\rightarrow 0$), which is underestimated. In fact, for the system in panel (i), the PA prediction for K is just barely larger than zero, turning to unphysical negative values when the volume fraction surpasses $\phi = 0.154$ at a fixed $n_s = 10^{-6}$ M. However, the PA-scheme values for d_s/d_0 remain in very good agreement with the ASD results, with a relative deviation of less than 3.5% even at $\phi = 0.15$. The values for d_s/d_0 predicted by the uncorrected $\delta\gamma$ scheme are generally in less good agreement with the simulation data, clearly revealed in Fig. 1 by the large-q offset of the corresponding $H(q)$.

The self-part corrected $\delta\gamma$-scheme results for $H(q)$ in Fig. 1 (red solid lines) illustrate that this hybrid scheme combines the good accuracy of the PA scheme regarding d_s, and of the $\delta\gamma$ scheme regarding $H^d(q)$. Indeed, the corrected $\delta\gamma$-scheme results for $H(q)$ are in overall good agreement with the ASD simulation data for all considered systems, with the largest deviation of 6% for $H(q_m)$ observed in panel (i).

In closing our discussion of Fig. 1, a short comment is in order regarding the computational cost caused by the considered methods of computing $H(q)$. The fast and accurate evaluation of $S(q)$ and $g(r)$ by the MPB-RMSA method, in combination with the easily evaluable integrals in Eqs. (14), (15), and (23), has allowed us to implement a convenient graphical user interface code, running on a standard desktop personal computer (PC). Using this code, MPB-RMSA results for $S(q)$ and $g(r)$, and PA-, $\delta\gamma$-, and self-part corrected $\delta\gamma$-scheme results for $H(q)$, are obtained in less than 1 second of central processing unit (cpu) time, for a given set of input parameters $\{L_B, \sigma, Z, n_s, \phi\}$. Thus, all curves depicted in Fig. 1, except for the ASD simulation data, have been obtained altogether in less than a minute on a standard desktop PC. In comparison, the computation of just one of the computer simulation curves in Fig. 1 required on a standard desktop PC typically 5 h of cpu time for generating 2000 equilibrated configurations (using our MC method) and approximately 8 h of cpu time for computing $H(q)$ with the ASD scheme. The overall accuracy and fast performance of the hybrid $\delta\gamma$ scheme in Eqs. (30)–(32) make this scheme well-suited for the real-time fitting of large sets of experimentally recorded data for $H(q)$ and $D(q)$.[56]

B. Hybrid $\delta\gamma$ scheme applied to neutral hard spheres

The main virtue of the d_s-corrected (zeroth-order) $\delta\gamma$ scheme lies in its good applicability to charge-stabilized systems. However, it is interesting to assess in more detail its performance in the limiting case of neutral hard spheres, in particular when the values of $H(q)$ at $q = 0$ and $q = q_m$ are considered. Recall for hard spheres that the accurate expression for d_s^{HS} in Eq. (31) should be preferentially used instead of the approximate PA result for larger $\phi \gtrsim 0.15$. For neutral spheres, higher-order HI contributions to d_s begin to matter at somewhat smaller concentrations than for charge-stabilized particles, where near-contact configurations are unlikely.

In Fig. 2, numerically precise lattice Boltzmann[50] and hydrodynamic force multipole simulation results[31] for $K^{\mathrm{HS}}(\phi)$ are compared with the predictions of all considered analytical schemes. For $\phi \lesssim 0.35$, the uncorrected $\delta\gamma$ scheme

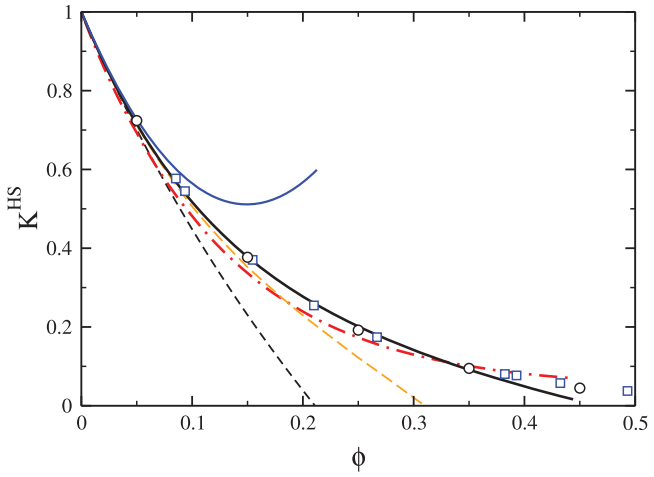

FIG. 2. Reduced short-time sedimentation coefficient, K^{HS}, of neutral colloidal hard spheres. Open circles: Hydrodynamic force multipole simulation data by Abade *et al.*[31] Open squares: lattice Boltzmann simulation data by Segrè *et al.*[50] Black dashed line: PA-scheme result. Dashed-dotted red line: uncorrected $\delta\gamma$-scheme result. Dashed orange line: self-part corrected $\delta\gamma$-scheme result in Eq. (30), with $[d_s/d_0]_{\mathrm{PA}}$ according to the PA-scheme result in Eq. (14). Solid black line: self-part corrected $\delta\gamma$-scheme result, using in place of $[d_s/d_0]_{\mathrm{PA}}$ the, for hard spheres, more accurate expression $[d_s/d_0]^{\mathrm{HS}}$ given in Eq. (31). Solid blue line: second-order virial result $K^{\mathrm{HS}} = 1 - 6.546\phi + 21.918\phi^2$ (see Ref. 38). The static structure factor input was calculated using the analytic Percus-Yevick solution.

underestimates the simulation data, showing the opposite trend of a slight overestimation for $\phi \gtrsim 0.35$. The corrected $\delta\gamma$ scheme with d_s-input according to Eq. (31), on the other hand, is in excellent agreement with the simulation data up to $\phi \approx 0.4$, reflecting the accuracy of the $\delta\gamma$-scheme predictions for $H^d(q)$ also for neutral spheres.

For large volume fractions $\phi \gtrsim 0.4$, however, the distinct part, $K^{\mathrm{HS}} - d_s^{\mathrm{HS}}/d_0$, of the sedimentation coefficient is considerably underestimated by the $\delta\gamma$ scheme, to such an extent that the self-part corrected $\delta\gamma$ scheme prediction for K^{HS} assumes unphysical negative values for $\phi \gtrsim 0.45$. Up to $\phi \approx 0.2$, the corrected $\delta\gamma$-scheme prediction for K^{HS}, with d_s^{HS} obtained by the PA scheme, lies closer to the simulation data than the uncorrected $\delta\gamma$-scheme result. This can be explained by the precise account of (two-body) lubrication effects in the PA-scheme, which are not included in the uncorrected $\delta\gamma$ scheme. At larger concentrations, however, the corrected $\delta\gamma$ scheme, with PA input for d_s, increasingly underestimates the sedimentation coefficient up to the point that, for $\phi \gtrsim 0.31$, unphysically negative values for K^{HS} are attained. This is a consequence of the already noted many-sphere hydrodynamic shielding effect, disregarded in the PA scheme, which lowers the strength of the HIs without reducing their range, leading to a larger self-diffusion coefficient than predicted on basis of hydrodynamic pair-interactions alone. The neglect of shielding effects by the PA scheme, both in the self- and distinct parts of K^{HS}, is the reason for the crossover of the PA curve of K^{HS} to negative values already at $\phi \approx 0.21$.

Regarding again Fig. 2, we finally note that the second-order virial result, $K^{\mathrm{HS}} = 1 - 6.546\phi + 21.918\phi^2 + \mathcal{O}(\phi^3)$, derived in[38] ceases to be applicable for $\phi \gtrsim 0.15$, where its curve bends up to larger values. This is the reason why this

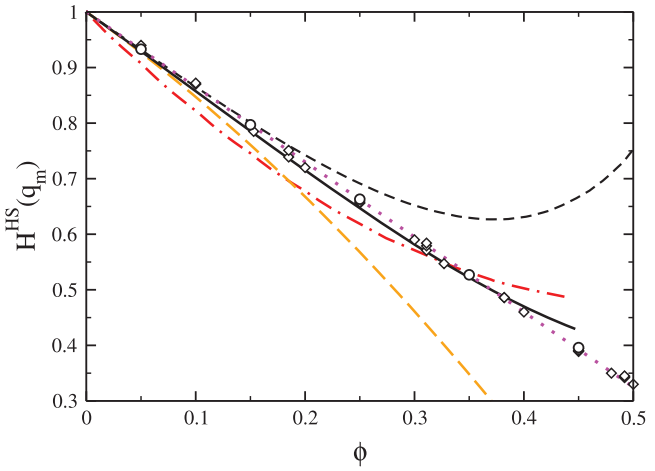

FIG. 3. Hydrodynamic function peak value, $H(q_m)$, of neutral hard spheres. Open circles: Hydrodynamic force multipole simulation results by Abade *et al.*[31] Open diamonds: ASD simulation data (see Ref. 14). Black dashed line and dashed-dotted red line: PA-scheme and uncorrected $\delta\gamma$-scheme results, respectively. Dashed orange line: self-part corrected $\delta\gamma$-scheme result in Eq. (30), with $[d_s/d_0]_{PA}$ calculated using the PA-scheme result in Eq. (14). Solid black line: self-part corrected $\delta\gamma$-scheme result, using in place of $[d_s/d_0]_{PA}$ for hard spheres the more accurate expression $[d_s/d_0]^{HS}$ given in Eq. (31). Dotted curve in violet: $1 - 1.35\phi$. The static structure factor input was obtained using the analytic Percus-Yevick solution.

second-order virial result cannot be used, different from the corresponding virial results for d_s^{HS}, η_∞^{HS}, and $H^{HS}(q_m)$, to construct analytic extrapolation formulas, valid for all concentrations up to the freezing transition.

We proceed by discussing the concentration dependence of the peak value, $H^{HS}(q_m)$, of the hydrodynamic function of neutral spheres. As noted in Sec. III, $H(q_m)$ is related to the short-time cage diffusion coefficient, $d_{cge} = d_0 H(q_m)/S(q_m)$, characterizing the initial decay rate of density fluctuations of wavelength equal to the next-neighbor cage size. Fig. 3 displays the decline of the hard-sphere $H(q_m)$ with increasing ϕ. To excellent accuracy up to the freezing volume fraction, this decline is described by the first-order virial result[14]

$$H^{HS}(q_m) = 1 - 1.35\phi. \tag{34}$$

Indeed, all the depicted ASD (Ref. 14) and hydrodynamic force multipole[31] values for $H(q_m)$ follow this line, indicating that, for a so far unknown reason, all higher order virial contributions cancel out. According to Fig. 3, the uncorrected $\delta\gamma$ scheme significantly underestimates $H^{HS}(q_m)$ for $\phi \lesssim 0.35$, overestimating it instead for $\phi \gtrsim 0.4$. In contrast, the corrected $\delta\gamma$-scheme result with the precise d_s^{HS} according to Eq. (31), is distinctly more accurate in that it only very slightly underestimates the linear decay in Eq. (34) for $\phi \lesssim 0.4$. Moreover, for $\phi > 0.4$, the positive-valued deviations from $1 - 1.35\phi$ are substantially smaller than those of the uncorrected $\delta\gamma$ scheme.

The corrected $\delta\gamma$-scheme prediction for $H^{HS}(q_m)$, with d_s calculated using the PA scheme, is a decent approximation up to $\phi \lesssim 0.15$. Its bending over to smaller values occurs for $H^{HS}(q_m)$ at somewhat larger ϕ values than in the sedimentation case, indicating that $\delta\gamma$-scheme results for $H^d(q)$ are more accurate at $q = q_m$ than at $q \approx 0$. The curve for $H^{HS}(q_m)$ predicted by the PA scheme bends over to larger values at a concentration $\phi \approx 0.37$ vastly beyond its range ($\phi \lesssim 0.1$) of applicability. The total neglect in the PA scheme of many-body HIs beyond the pair level implies, at larger ϕ, an underestimation of d_s, but to a larger extent an overestimation of $H^d(q_m)$. As a net result, $H^{HS}(q_m)$ at large ϕ is strongly overestimated by the PA scheme.

In summarizing our discussion of hard-sphere systems, the key message conveyed by Figs. 2 and 3 is that the corrected $\delta\gamma$ scheme, with d_s according to Eq. (31), describes $H^{HS}(q)$ quite precisely for $\phi \lesssim 0.4$. It can be applied to reasonable accuracy even to larger ϕ values, with the exception of small q values.

C. High-frequency viscosity

In this Subsection, we compare viscosity results obtained by the various methods described in Sec. IV, for the two limiting cases of deionized (low-salinity) charged-sphere and neutral hard-sphere suspensions. Results for systems with intermediate added salt are bracketed by these two limiting cases.

In Fig. 4, we display our viscosity results for neutral hard spheres with those for two deionized suspensions of highly charged spheres (CS) where $n_s = 0$. Results by all the methods in Sec.IV are shown. We point out that, in addition to the CS system of Fig. 1 with parameters $L_B = 5.617$ nm, $\sigma = 200$ nm, and $Z = 100$ (referred to here as system CS-1), whose ASD results for η_∞ in Fig. 4 are indicated by filled red circles, we additionally show viscosity results for another zero-salt system where $L_B = 0.71$ nm, $\sigma = 50$ nm, and $Z = 70$ (labeled CS-2), whose ASD data for η_∞ are represented by red diamonds filled in blue. The reason for including in Fig. 4 results for two different deionized systems, is that system CS-1 freezes at $\phi \approx 0.15$, whereas system CS-2 stays fluid up to $\phi \sim 0.3$, allowing us to test the predictions of our analytical methods in a more extended volume fraction range. The ASD simulation data for $\eta_\infty(\phi)$ for systems CS-1 and CS-2 merge continuously, overlapping nearly perfectly within $0.1 < \phi < 0.15$. This indicates that the limiting behavior of η_∞ for highly correlated charged spheres is practically reached in both systems. Therefore, the depicted CS-results for η_∞ were calculated in the analytic schemes using the parameters of system CS-2 only. The deviations in η_∞ for the two CS systems are minuscule in all considered analytic schemes.

Consider first the performance of the PA scheme. By its definition, the PA result for η_∞ is in very good agreement with the ASD simulation data at low ϕ, but the agreement becomes poorer with increasing volume fraction. While the deviations between the ASD and PA results for low-salt systems are very small up to $\phi \lesssim 0.2$, for neutral spheres significant differences are visible already for $\phi \gtrsim 0.1$. These differences originate from the fact that in charged-sphere suspensions, near-contact configurations are disfavored by the electric repulsion, i.e., charged-sphere systems are hydrodynamically more dilute than neutral sphere suspensions. Since higher-order HI effects on η_∞ in low-salinity charged systems are weaker, for many such systems (including system CS-1), which freeze already at $\phi \lesssim 0.2$, the accuracy of the PA-scheme for η_∞ is sufficiently good in the whole fluid regime. Regarding $H(q)$,

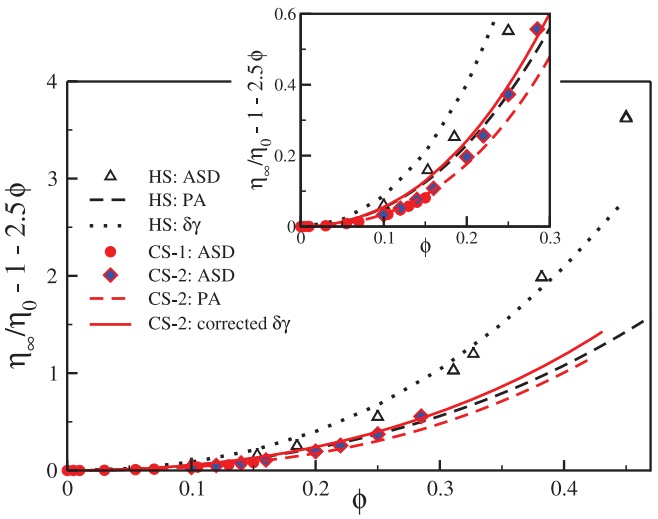

FIG. 4. Reduced high-frequency viscosity, η_∞/η_0, as a function of ϕ, for a suspension of neutral hard spheres (HS, in black), and two deionized charged-sphere suspensions (CS-1 and CS-2, in red). The leading-order Einstein contribution, $1 + 2.5\phi$, is subtracted off to expose the differences. Symbols: ASD simulation results. Dashed lines: PA-scheme results according to Eq. (18). Dotted lines: $\delta\gamma$-scheme results according to Eqs. (24)–(26). Solid lines: self-part corrected $\delta\gamma$-scheme results according to Eqs. (32), (25), and (26). All analytic schemes use the MPB-RMSA $S(q)$ as input. The CS-1 viscosity results represented by red filled circles are ASD data for $L_B = 5.617$ nm, $\sigma = 200$ nm, and $Z = 100$. The ASD data for the more weakly charged, smaller particles of system CS-2, with $L_B = 0.71$ nm, $\sigma = 50$ nm, and $Z = 70$ are indicated by red diamonds filled in blue. The parameters of system CS-2 have been used in the analytic calculations. The inset magnifies the details at lower ϕ.

however, the PA-scheme predictions for charged spheres deviate significantly from the ASD data already at $\phi = 0.105$ (see again Fig. 1). At larger ϕ, and in contrast to the ASD data, the PA scheme predicts only a slight enlargement of η_∞ in going from charged to neutral spheres. The distinctly larger values of η_∞ for concentrated hard-sphere suspensions are thus mostly due to near-field, many-body HIs which enlarge the viscous dissipation. Overall, however, η_∞ is rather insensitive to the range of the pair potential, at least in comparison to the static (zero frequency) viscosity which for concentrated systems can become very much larger than η_∞.[57]

The self-part modified $\delta\gamma$ scheme for η_∞, defined by Eq. (32), agrees overall very well with the ASD data for charged spheres in the whole fluid-state concentration regime. Small deviations from the simulation data are noticed at low ϕ values only. Regarding neutral hard spheres, a similar observation applies to the unmodified second-order $\delta\gamma$ scheme, which describes the ASD simulation data quite well up to $\phi \approx 0.4$. The slight overestimation of $\eta_\infty^{\mathrm{HS}}$ at lower ϕ can be attributed to the non-exact treatment of two-body HI contributions by the $\delta\gamma$ scheme.

Overall, the high-frequency viscosity of charged-sphere systems at low salinity is well captured by the modified $\delta\gamma$-scheme in Eq. (32), and for neutral hard spheres by the unmodified $\delta\gamma$ scheme (up to $\phi \approx 0.4$). Different from the self-part corrected $\delta\gamma$ scheme for $H(q)$, which makes reliable predictions for arbitrary salinities, the modified $\delta\gamma$ scheme for η_∞ applies to low-salinity systems only, and the unmodified $\delta\gamma$ scheme only to neutral hard spheres. The reasons for this have been discussed already in Subsection IV C.

Before closing our discussion of η_∞, it is of interest to compare the numerical efforts required by the employed methods. The computation of the 45 ASD data points for neutral and charged spheres included in Fig. 4 required about 500 h of cpu time on a modern desktop PC. This large time investment should be compared to the few minutes computation time on a comparable PC which were required for the results by all considered analytic schemes, amounting to more than one thousand data points on a dense mesh of ϕ values.

VI. RELATION BETWEEN VISCOSITY AND DIFFUSION PROPERTIES

Having quite accurate analytic methods for short-time properties at our disposal, we are in the position to analyze possible relations between these properties in the whole fluid-state concentration regime. Specifically, we want to test the validity of two GSE relations,

$$\frac{D^*(\phi)}{d_0} \times \frac{\eta_\infty(\phi)}{\eta_0} \approx 1, \tag{35}$$

for $D^*(\phi) = d_s(\phi)$ and $D^*(\phi) = d_{\mathrm{cge}}(\phi)$. In addition, we probe the validity of the Kholodenko-Douglas GSE (KD-GSE) relation,[58]

$$\frac{d_c(\phi)}{d_0} \times \frac{\eta_\infty(\phi)}{\eta_0} \times \sqrt{S(q \to 0, \phi)} \approx 1, \tag{36}$$

between the collective diffusion coefficient, $d_c = K/S(q \to 0)$, η_∞, and the square root of the isothermal osmotic compressibility given by $S(q \to 0)$. In particular, the KD-GSE relation has been used in various biophysical and soft matter studies.[59–62]

All three considered GSE relations are exact at $\phi = 0$ only. The approximate validity of a GSE relation in concentrated systems is an important issue in microrheological studies, since this allows to infer a rheological property more easily from a diffusion measurement. For testing the GSE relations in Eqs. (35) and (36), we consider here again the two limiting HSY cases of a low-salinity charge-stabilized system and neutral spheres, since the differences in the respective short-time dynamic properties are here largest.

For a precise test of the GSE relations in the case of hard spheres, we take advantage of simple analytic expressions available for all short-time properties appearing in Eqs. (35) and (36), with the exception of K, for which we use the quite accurate self-part corrected $\delta\gamma$-scheme result depicted in Fig. 2. The analytic expressions for hard spheres, which apply to excellent accuracy up to $\phi = 0.5$, are Eq. (34) for $H^{\mathrm{HS}}(q_m)$, Eq. (31) for d_s^{HS}, and the generalized Saitô-type expression for $\eta_\infty^{\mathrm{HS}}$,[32]

$$\frac{\eta_\infty^{\mathrm{HS}}}{\eta_0} = 1 + \frac{5}{2}\phi\frac{1+S}{1-\phi(1+S)}, \tag{37}$$

where $S = 1.001\phi + 0.95\phi^2 - 2.15\phi^3$. Moreover, we use the precise formula[57] for the structure factor peak height,

$$S^{HS}(q_m) \approx 1 + 0.644\phi g^{HS}(x = 1^+), \tag{38}$$

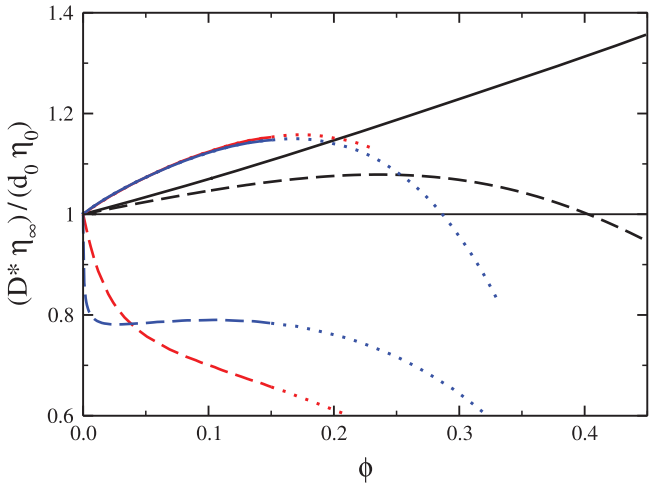

FIG. 5. Test of the two GSE relations in Eq. (35), relating η_∞ to d_s and $d_{\rm cge}$, respectively. Solid lines: $(d_s/d_0) \times (\eta_\infty/\eta_0)$ vs. ϕ. Dashed lines: $(d_{\rm cge}/d_0) \times (\eta_\infty/\eta_0)$ vs. ϕ. Black curves are hard-sphere results obtained from Eqs. (31), (34), (37), and (38). Red and blue curves are corrected $\delta\gamma$-scheme results for the low-salinity charged-sphere systems CS-1 and CS-2, respectively, both assuming a residual salt content of $n_s = 10^{-6}$ M. The corrected $\delta\gamma$-scheme results have been calculated using Eqs. (32), (25), and (26) for η_∞, and Eqs. (30) and (14) for d_s and $d_{\rm cge} = d_0 H(q_m)/S(q_m)$. As input to all analytic schemes, MPB-RMSA results for $S(q)$ have been used.

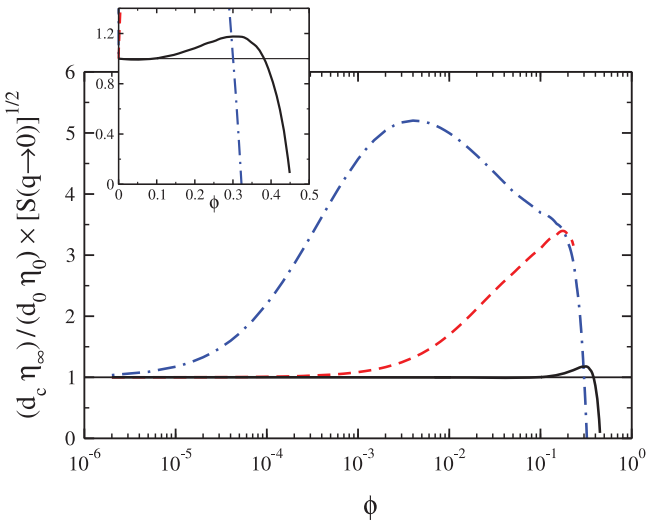

FIG. 6. Test of Kholodenko-Douglas GSE relation in Eq. (36). Black curves: neutral hard-sphere results based on the precise analytic result in Eq. (37) for $\eta_\infty^{\rm HS}$, $S^{\rm HS}(q \to 0)$ according to the Carnahan-Starling equation of state, and $K^{\rm HS}$ calculated by the self-part corrected $\delta\gamma$-scheme Eq. (30), using in place of $[d_s/d_0]_{\rm PA}$ the, for hard spheres, more accurate expression $[d_s/d_0]^{\rm HS}$ given in Eq. (31). Red (dashed) and blue (dashed-dotted) curves are self-part corrected $\delta\gamma$-scheme results for the low-salinity systems CS-1 and CS-2 (with $n_s = 10^{-6}$ M), respectively, using Eqs. (32), (25), and (26) for η_∞, and Eqs. (30) and (14) for $d_c = d_0 H(q \to 0)/S(q \to 0)$. As input to all analytic schemes, MPB-RMSA results for $S(q)$ have been used.

where $g^{HS}(x = 1^+) = (1 - 0.5\phi)/(1 - \phi)^3$ is the Carnahan-Starling contact value for the hard-sphere rdf. For $S^{\rm HS}(q \to 0)$ in Eq. (36), we employ the Carnahan-Starling equation of state.[22]

In testing the GSE relations in Eqs. (35) and (36) for low-salinity systems, for the diffusion properties we use the self-part corrected $\delta\gamma$ scheme, with d_s calculated by the PA scheme. For η_∞ we use the corrected $\delta\gamma$ scheme according to Eq. (32).

The validity of the two GSE relations in Eq. (35) is examined in Fig. 5. A valid GSE relation is reflected by a horizontal line of unit height. For neutral hard spheres (black lines), the product $(d_s^{\rm HS}/d_0) \times (\eta_\infty^{\rm HS}/\eta_0)$ is well approximated, for all displayed ϕ, by its first-order in ϕ expansion given by $1 + 0.67\phi$, showing a more than 20% violation of this GSE relation for $d_s^{\rm HS}$ when $\phi \gtrsim 0.3$.

Different from $d_s^{\rm HS}$, the GSE scaling for $d_{\rm cge}^{\rm HS}$ is approximately satisfied with a maximal deviation from one of 8%. Thus, for hard-sphere like colloidal particles available only in amounts too small for a mechanical rheological experiment, one can determine η_∞ approximately from a dynamic scattering experiment measuring $D(q_m)$.

According to Fig. 5, in low-salinity systems of charged particles, the GSE-relation for d_s is overall of similar accuracy as that for hard spheres, although the deviations from one are larger at smaller ϕ. The curves for $(d_s/d_0) \times (\eta_\infty/\eta_0)$ obtained for the two low-salinity systems coincide practically for $\phi \lesssim 0.15$. The downturn of these two curves at larger $\phi \gtrsim 0.18$, indicated by the dotted curve continuations in Fig. 5, is not shared by the ASD simulation data (cf., Fig. 25 in Ref. 14). This is an artifact of the PA scheme which, as discussed already in relation to Fig. 1, tends to underestimate d_s at larger ϕ.

Different from neutral hard spheres, in low-salinity systems the GSE relation for $d_{\rm cge}$ is manifestly violated already at very low ϕ. The strong difference in the $(d_{\rm cge}/d_0) \times (\eta_\infty/\eta_0)$ curves for the two considered low-salinity systems is due to the different ϕ-dependence of their respective $S(q_m)$. The pronounced decline of both curves at low ϕ is mainly triggered by the sharp low-ϕ rise of $S(q_m)$ in low-salinity systems.

Kholodenko and Douglas[58] have proposed the GSE relation in Eq. (36) using mode-coupling theory like arguments. For neutral spheres at low ϕ, we can check this relation analytically using the numerically precise second-order virial expansion results for $K^{\rm HS}$ in Ref. 38, $\eta_\infty^{\rm HS}$ in Ref. 39, and $S^{\rm HS}(q \to 0)$ given by the Carnahan-Starling equation of state. This leads to

$$\frac{d_C^{\rm HS}}{d_0} \times \frac{\eta_\infty^{\rm HS}}{\eta_0} \times \sqrt{S^{\rm HS}(q \to 0, \phi)} = 1 - 0.046\phi + 1.3713\phi^2 + \mathcal{O}(\phi^3), \tag{39}$$

where the first-order virial coefficient is indeed close to zero. Using the analytic expressions for $\eta_\infty^{\rm HS}$ in Eq. (37), and $K^{\rm HS}$ calculated in the self-part corrected $\delta\gamma$-scheme with d_s according to Eq. (31), we can test the KD-GSE relation in fact in the full fluid-state regime of neutral spheres. According to the inset in Fig. 6, the KD-GSE for neutral spheres is valid to decent accuracy up to $\phi \lesssim 0.4$, with a maximal positive-valued deviation from one at $\phi \approx 0.3$ of less than 18%. Strong negative-valued deviations from one are observed for $\phi \gtrsim 0.4$, where the KD-GSE relation ceases to be applicable to neutral hard spheres.

The corrected $\delta\gamma$-scheme results included in Fig. 6 demonstrate the striking violation of the KD-GSE relation, when low-salinity systems of charged particles are considered. A clear violation of this relation is observed for all concentrations $\phi \gtrsim 10^{-4}$ in the case of the low-salinity system CS-1, and for $\phi \gtrsim 10^{-2}$ in the case of system CS-2, where, for both systems, a residual salt concentration of $n_s = 10^{-6}$ M has been assumed. The maximal (positive-valued) violation of the KD-GSE relation occurs roughly at a volume fraction where the $d_c(\phi)$ of charged spheres attains its maximum. The maximum in $d_c(\phi)$, in turn, is the result of a competition, with increasing ϕ, between decreasing compressibility and decreasing sedimentation coefficient. The concentration at the peak of $d_c(\phi)$ is determined roughly from $k_c^2(\phi) = k_s^2$.[5] The downturn of the $d_c\eta_\infty\sqrt{S(q \to 0)}/(d_0\eta_0)$ curve at large ϕ, observable in Fig. 6 for neutral and charged spheres alike, is triggered by the large-ϕ decline both of K and η_∞.

VII. CONCLUSIONS

We have presented a comprehensive theoretical and computer simulation study of short-time dynamic properties of colloidal spheres, interacting by a HSY pair potential. In this study, the accuracy of essentially analytic and very fast methods of calculating $H(q)$, d_s, and η_∞ has been explored in comparison with numerically expensive ASD simulation results, obtained as functions of volume fraction and added salt content. We have been particularly concerned with the low screening (low salinity) and infinite screening (i.e., neutral sphere) limits of the HSY model.

The static pair functions $S(q)$ and $g(r)$, required as the only input to the PA and (self-part corrected) $\delta\gamma$ schemes, have been determined using our recently developed MPB-RMSA method. The PA scheme, which precisely (and only) accounts for two-body HIs, is for arbitrary salt concentration in excellent agreement with the simulation data for $H(q)$, provided that $\phi \lesssim 0.1$. With regard to the high-frequency viscosity, the PA-scheme predictions are in good agreement with the simulation data for volume fractions up to $\phi \approx 0.1$ for neutral hard spheres, and up to $\phi \approx 0.2$ for strongly charged spheres in the weak screening (low salinity) regime. At larger ϕ, three-body and higher-order HIs become influential.

The self-part corrected $\delta\gamma$ scheme for $H(q)$ is in good agreement with our ASD results for the hydrodynamic function of charged spheres at all considered ϕ and n_s values. When the self-part corrected $\delta\gamma$ scheme is applied to neutral hard spheres, using d_s^{HS} according to Eq. (31), also $H^{\mathrm{HS}}(q)$ is predicted to very good accuracy even up to $\phi \approx 0.4$, including the small-q region.

We have shown that the (second-order) $\delta\gamma$-scheme expression for η_∞, given by Eqs. (24)–(26), is only applicable to hard-sphere like systems (i.e., at large screening). Its predictions for $\eta_\infty^{\mathrm{HS}}$, however, agree well with the ASD data up to $\phi \lesssim 0.4$. At larger ϕ, it underestimates the high-frequency viscosity. Based on arguments applying to low-salinity charge-stabilized systems only, we have introduced in Eq. (32) a simple correction to the $\delta\gamma$-scheme result for η_∞. This corrected $\delta\gamma$ scheme predicts to good accuracy the high-frequency viscosity of low-salinity systems, even up to the freezing concentration. Different from the self-part corrected $\delta\gamma$ scheme for $H(q)$ introduced in Eq. (30), which applies at any salt concentration under the condition that $\phi \lesssim 0.15$, the corrected $\delta\gamma$ scheme for η_∞ in Eq. (32) is valid at low salinities only. An appropriately corrected $\delta\gamma$ scheme for η_∞, applicable for arbitrary salinities, is still missing. Its development could be the topic of a future study.

An interesting application of the hybrid $\delta\gamma$ schemes for $H(q)$ and η_∞ has been our validity tests of three approximate generalized Stokes-Einstein relations linking η_∞ to d_s, d_{cge}, and d_c, respectively. For an optimal test of these relations in the special case of neutral hard spheres, precise analytic expressions for d_s^{HS}, $H^{\mathrm{HS}}(q_m)$, $S^{\mathrm{HS}}(q_m)$, and $S^{\mathrm{HS}}(q \to 0)$ have been used, valid in the whole fluid-state concentration range. The key finding from our validity tests of GSE relations is the strong dependence of their accuracies on the range and character of the particle interactions. The most striking example in case is the Kholodenko-Douglas GSE relation, which applies decently well to neutral spheres up to $\phi \approx 0.4$. The very same relation, however, is strongly violated in low-salinity suspensions already at very low volume fractions.

ACKNOWLEDGMENTS

M.H. acknowledges support by the International Helmholtz Research School of Biophysics and Soft Matter (IHRS BioSoft). A.J.B. acknowledges financial support from SeCyT-UNC and CONICET. This work was under appropriation of funds from the Deutsche Forschungsgemeinschaft (DFG) (SFB-TR6, project B2).

[1] W. B. Russel, D. A. Saville, and W. R. Schowalter, *Colloidal Dispersions* (Cambridge University Press, Cambridge, England, 1989).
[2] D. O. Riese, G. H. Wegdam, W. L. Vos, R. Sprik, D. Fenistein, J. H. H. Bongaerts, and G. Grübel, Phys. Rev. Lett. **85**, 5460 (2000).
[3] P. Holmqvist and G. Nägele, Phys. Rev. Lett. **104**, 058301 (2010).
[4] J. Gapinski, A. Wilk, A. Patkowski, W. Häussler, A. J. Banchio, R. Pecora, and G. Nägele, J. Chem. Phys. **123**, 054708 (2005).
[5] M. Heinen, F. Zanini, F. Roosen-Runge, D. Fedunová, F. Zhang, M. Hennig, T. Seydel, R. Schweins, M. Sztucki, M. Antalík, F. Schreiber, and G. Nägele, "Viscosity and diffusion: Crowding and salt effects in protein solutions," Soft Matter (submitted).
[6] F. Roosen-Runge, M. Hennig, F. Zhang, R. M. J. Jacobs, M. Sztucki, H. Schober, T. Seydel, and F. Schreiber, Proc. Natl. Acad. Sci. U.S.A. **108**, 11815 (2011).
[7] E. J. W. Verwey and J. T. G. Overbeek, *Theory of the Stability of Lyophobic Colloids* (Elsevier, New York, 1948).
[8] P. N. Pusey, *Liquids, Freezing and the Glass Transition* (Elsevier, Amsterdam, 1991).
[9] M. Heinen, P. Holmqvist, A. J. Banchio, and G. Nägele, J. Appl. Crystallogr. **43**, 970 (2010).
[10] A. J. Banchio, J. Gapinski, A. Patkowski, W. Häussler, A. Fluerasu, S. Sacanna, P. Holmqvist, G. Meier, M. P. Lettinga, and G. Nägele, Phys. Rev. Lett. **96**, 138303 (2006).
[11] W. Häussler and B. Farago, J. Phys. Condens. Matter **15**, S197 (2003).
[12] C. Le Coeur and S. Longeville, Chem. Phys. **345**, 298 (2008).
[13] T. M. Squires and T. G. Mason, Annu. Rev. Fluid Mech. **42**, 413 (2010).
[14] A. J. Banchio and G. Nägele, J. Chem. Phys. **128**, 104903 (2008).
[15] C. W. J. Beenakker and P. Mazur, Physica A **126**, 349 (1984).
[16] C. W. J. Beenakker and P. Mazur, Physica A **120**, 388 (1983).
[17] C. W. J. Beenakker, Physica A **128**, 48 (1984).
[18] M. Heinen, P. Holmqvist, A. J. Banchio, and G. Nägele, J. Chem. Phys. **134**, 044532 (2011).
[19] M. Heinen, P. Holmqvist, A. J. Banchio, and G. Nägele, J. Chem. Phys. **134**, 129901 (2011).
[20] W. B. Russel and D. W. Benzing, J. Colloid Interface Sci. **83**, 163 (1981).

[21]A. R. Denton, Phys. Rev. E **62**, 3855 (2000).
[22]J.-P. Hansen and I. R. McDonald, *Theory of Simple Liquids*, 2nd ed. (Academic, London, 1986).
[23]F. J. Rogers and D. A. Young, Phys. Rev. A **30**, 999 (1984).
[24]J. K. Percus and G. J. Yevick, Phys. Rev. **110**, 1 (1958).
[25]M. S. Wertheim, Phys. Rev. Lett. **10**, 321 (1963).
[26]G. Nägele, Phys. Rep. **272**, 215 (1996).
[27]J. K. G. Dhont, *An Introduction to Dynamics of Colloids* (Elsevier, Amsterdam, 1996).
[28]R. B. Jones and P. N. Pusey, Annu. Rev. Phys. Chem. **42**, 137 (1991).
[29]P. Szymczak and B. Cichocki, J. Stat. Mech: Theory Exp. P01025 (2008).
[30]A. J. Banchio and J. F. Brady, J. Chem. Phys. **118**, 10323 (2003).
[31]G. C. Abade, B. Cichocki, M. L. Ekiel-Jeżewska, G. Nägele, and E. Wajnryb, J. Chem. Phys. **132**, 014503 (2010).
[32]G. C. Abade, B. Cichocki, M. L. Ekiel-Jeżewska, G. Nägele, and E. Wajnryb, J. Chem. Phys. **133**, 084906 (2010).
[33]D. J. Jeffrey and Y. Onishi, J. Fluid Mech. **139**, 261 (1984).
[34]R. B. Jones and R. Schmitz, Physica A **149**, 373 (1988).
[35]G. K. Batchelor and J. T. Green J. Fluid Mech. **56**, 401 (1972).
[36]W. B. Russel, J. Chem. Soc., Faraday Trans. **80**, 31 (1984).
[37]B. Cichocki, M. L. Ekiel-Jezewska, and E. Wajnryb, J. Chem. Phys. **111**, 3265 (1999).
[38]B. Cichocki, M. L. Ekiel-Jezewska, P. Szymczak, and E. Wajnryb, J. Chem. Phys. **117**, 1231 (2002).
[39]B. Cichocki, M. L. Ekiel-Jezewska, and E. Wajnryb, J. Chem. Phys. **119**, 606 (2003).
[40]U. Genz and R. Klein, Physica A **171**, 26 (1991).
[41]A. J. Banchio, J. Gapinski, A. Patkowski, W. Häussler, A. Fluerasu, S. Sacanna, P. Holmqvist, G. Meier, M. P. Lettinga, and G. Nägele, Phys. Rev. Lett. **96**, 138303 (2006).
[42]E. Overbeck, C. Sinn, and M. Watzlawek, Phys. Rev. E **60**, 1936 (1999).
[43]G. Nägele, B. Steininger, U. Genz, and R. Klein, Phys. Scr. **55**, 119 (1994).
[44]G. Nägele, B. Mandl, and R. Klein, Prog. Coll. Polym. Sci. **98**, 117 (1995).
[45]M. Watzlawek and G. Nägele, J. Colloid Interface Sci. **214**, 170 (1999).
[46]G. C. Abade, B. Cichocki, M. L. Ekiel-Jeżewska, G. Nägele, and E. Wajnryb, J. Chem. Phys. **134**, 244903 (2011).
[47]F. M. Horn, W. Richtering, J. Bergenholtz, N. Willenbacher, and N. J. Wagner, J. Colloid Interface Sci. **225**, 166 (2000).
[48]A. J. C. Ladd, J. Chem. Phys. **93**, 3484 (1990).
[49]G. Mo and A. S. Sangani, Phys. Fluids **6**, 1637 (1994).
[50]P. N. Segrè, O. P. Behrend, and P. N. Pusey, Phys. Rev. E **52**, 5070 (1995).
[51]A. J. C Ladd, H. Gang, J. X. Zhu, and D. A. Weitz, Phys. Rev. E **52**, 6550 (1995).
[52]M. J. Stevens and M. O. Robbins, J. Chem. Phys. **98**, 2319–2324 (1993).
[53]J.-P. Hansen and L. Verlet, Phys. Rev. **184**, 151 (1969).
[54]K. Kremer, M. O. Robbins, and G. S. Grest, Phys. Rev. Lett. **57**, 2694 (1986).
[55]J. Gapinski, A. Patkowski, and G. Nägele, J. Chem. Phys. **132**, 054510 (2010).
[56]M. Heinen, P. Holmqvist, A. J. Banchio, and G. Nägele, "Short- and long-time dynamics of charged colloidal particles," (in preparation).
[57]A. J. Banchio, G. Nägele, and J. Bergenholtz, J. Chem. Phys. **111**, 8721 (1999).
[58]A. L. Kholodenko and J. F. Douglas, Phys. Rev. E **51**, 1081 (1995).
[59]A. K. Gaigalas, V. Reipa, J. B. Hubbard, J. Edwards, and J. Douglas, Chem. Eng. Sci. **50**, 1107 (1995).
[60]D. E. Cohen, G. M. Thurston, R. A. Chamberlin, G. B. Benedek, and M. C. Carey, Biochemistry **37**, 14798 (1998).
[61]P. Boogerd, B. Scarlett, and R. Brouwer, Irrig. Drain. **50**, 109 (2001).
[62]F. Nettesheim, M. W. Liberatore, T. K. Hodgdon, N. J. Wagner, E. W. Kaler, and M. Vethamuthu, Langmuir **24**, 7718 (2008).